Electronic Supplementary Material (ESI) for Journal of Materials Chemistry A.

Supplementary information

Boosting C_2H_2/CO_2 Separation of Metal-Organic Frameworks via Anion Exchange and Elevating Temperature

Ting Wang,[a#] Wei Mei,[b#] Pengfei Li,[a,c#] Yun-Lei Peng,[a] Yao Chen,[e] Jian-Gong Ma,[a] Peng Cheng,[ad] Ming Fang,[c*] Kuang Yu,[b*] Zhenjie Zhang[ade*]

Single Crystal X-ray diffraction structure analysis

Single crystal diffraction data of **NKMOF-2-BF$_4$** were collected at 120 K under an Oxford Cryo stream system on a SuperNova (Mo) X-ray Source with micro-focus sealed X-ray tube. The structures were solved using the direct method and refined with the full-matrix least-squares technique using the 'XS' and 'XL' program package. Due to the presence of highly disordered guest molecules in the pore, "SQUEEZE" operation of Platon software was applied to all seven sets of crystal data. All nonhydrogen atoms were refined with anisotropic displacement parameters. The hydrogen atoms on the ligands were placed in idealized positions and refined using a riding model. Hydrogen in μ_3-OH is added by hydrogenated manually, and the distance between hydrogen and oxygen and copper atoms are limited by DFIX instructions. The detailed crystallographic data and structure refinement parameters are summarized in Table S1 (CCDC: 1982349)

Fitting of single-component adsorption isotherms

The single-component adsorption isotherms for C_2H_2 and CO_2 in **NKMOF-2-Cl** and **NKMOF-2-BF$_4$** were determined by fitting the adsorption isotherms at 298 K for the respective adsorbates to the dual-site Langmuir–Freundlich (DSLF) equation,[1] The DSLF equation was given by:

$$q = q_{A,sat}\frac{b_A P^{n_A}}{1 + b_A P^{n_A}} + q_{B,sat}\frac{b_B P^{n_B}}{1 + b_B P^{n_B}}$$

where q is the uptake (in mmol g^{-1}), P is the pressure (in kPa), $q_{A,sat}$ and $q_{B,sat}$ are the saturation uptakes (in mmol g^{-1}) for sites 1 and 2, b_A and b_B are the affinity coefficients (in kPa^{-1}) for sites 1 and 2, and n_A and n_B represent the deviations from the ideal homogeneous surface. The single-component adsorption isotherms for C_2H_2 and CO_2 were fitted by the above form of DSLF equation.[2] The fitting parameters were displayed in **Table S6-7**.

Isosteric Heat of Adsorption

A virial-type expression comprising the temperature-independent parameters a_i and b_j was employed to calculate the enthalpies of adsorption for CO_2 and C_2H_2 (at 273 K and 298 K) on **NKMOF-2-Cl** and **NKMOF-2-BF_4**. In each case, the data were fitted use equation：

$$LnP = LnN + \frac{1}{T}\sum_{i=0}^{m} a_i N^i + \sum_{j=0}^{n} b_j N^j$$

$$Q_{st} = -R\sum_{i=0}^{m} a_i N^i$$

Here, P is the pressure expressed in bar, N is the amount absorbed in mmol g^{-1}, T is the temperature in K, a_i and b_j are virial coefficients, and m, n represent the number of coefficients required to adequately describe the isotherms (m and n were gradually increased till the contribution of extra added a and b coefficients was deemed to be statistically insignificant towards the overall fit. And the average value of the squared deviations from the experimental values was minimized).

Q_{st} is the coverage-dependent isosteric heat of adsorption and R is the universal gas

constant. The heat enthalpy of gas sorption for **NKMOF-2-Cl** and **NKMOF-2-BF_4** in this manuscript are determined by using the sorption data measured in the pressure range from 0 - 1 bar (273 K and 298 K).

IAST selectivity calculation

In order to compare the C_2H_2/CO_2 separation performance of various MOFs, IAST calculations of mixture adsorption were performed. For separation of a binary mixture of components A and B, the adsorption selectivity is defined by

$$S_{abs} = \frac{q_A / q_B}{y_A / y_B}$$

Calculation of the kinetic amount based on breakthrough curves

The gas adsorption capacity during the breakthrough experiments was calculated by the following equations:[3]

$$q_i = \frac{C_i V}{m} \times \int_0^t (1 - \frac{F}{F_0}) dt$$

Where q_i is the equilibrium adsorption capacity of gas i ($cm^3\ g^{-1}$), C_i is the feed gas concentration, V is the volumetric feed flow rate ($cm^3\ min^{-1}$), t is the adsorption time (min), F_0 and F are the inlet and outlet gas molar flow rates, respectively, and m is the mass of the adsorbent (g).

Computational Details

All the Density Functional Theory (DFT) simulations were performed using the Vienna ab initio simulation package (VASP) in conjunction with the van der Waals (*vdw*) corrected optPBE-*vdW* functional and the projector augmented wave (PAW) method.[4-8] A Hubbard-type on-site U correction was applied on the Cu *d* states, with the U and J parameters setting to 8 and 1 eV, respectively.[9] The energy cutoff on the wave function was set to 400 eV. We used only the gamma point to sample the Brillouin Zone, which is a reasonable scheme for studying insulators with large unit cells. All the geometry optimizations were performed using a 10^{-4} eV/atom energy threshold, and all forces were converged within 0.01 eV/Å.

Due to Pulay stress, **NKMOF-2** cannot be optimized directly as it will collapse into unphysical nonporous geometries. Therefore, we applied an artificial anisotropic internal stress to counterbalance the artifacts caused by Pulay stress. We gradually increase the magnitude of the artificial internal stress, so the box volume expands correspondingly. The optimal box dimensions and geometry were obtained when the lattice energy (without the artificial PV term) reaches its minimum. The lattice energy change with respect to the internal stress are shown in **Fig. S18**. The internal stress corresponding to the minimal energy of **NKMOF-2-Cl** and **NKMOF-2-BF_4** was 20 and 27.5 kbar, respectively. Both the obtained structures of **NKMOF-2-Cl** and **NKMOF-2-BF_4** corresponding to the minimum energy are in excellent agreement with

the experimental results.

Density functional theory (DFT) calculations are performed to understand the reasons for the increased loading of **NKMOF-2-BF_4**, as well as its adsorption selectivity. We first optimize the structures of empty **NKMOF-2-Cl** and **NKMOF-2-BF_4** without guest molecules. By exerting additional isotropic stress, we remove the pulay stress artifacts and obtain the optimal geometry of empty **NKMOF-2-Cl** and **NKMOF-2-BF_4** (see SI for details). The resulted lattice parameters are listed in **Table S8**, in comparison with the experimental data. Excellent agreement between experiment and calculation is achieved, with deviations smaller than 3.1% for **NKMOF-2-Cl** and 1.8% for **NKMOF-2-BF_4**, validating our calculation methods.

To further verified that we did not under sample **NKMOF-2-Cl**, we transfer the CO_2 geometries of all four sites in **NKMOF-2-BF_4** into the **NKMOF-2-Cl** frame, fixing their relative orientations for the Cu-O skeleton. Then we reoptimize and compute the resulted adsorption energies, and compare them with their counterparts in **NKMOF-2-BF_4**. The results are shown in **Table S9**, only site I remains low energy in **NKMOF-2-Cl**, while all other three sites become much less stable. Therefore, **NKMOF-2-BF_4** does possess much more low-energy sites compare to **NKMOF-2-Cl**, validating our conclusion.

Starting from the optimal structure, we insert CO_2 molecule randomly into the **NKMOF-2-Cl** and **NKMOF-2-BF_4**, keeping the distance between the CO_2 and the framework atoms larger than 2.5Å. We sample 20 different initial geometries for CO_2 in **NKMOF-2-Cl** and **NKMOF-2-BF_4**, respectively. After the guest molecule is

inserted, we fix the lattice parameters and only optimize the atom positions. Meanwhile, the energy of a single CO_2 is computed using an empty box with the same dimension as the optimized **NKMOF-2**.

The interaction energy between CO_2, anion (BF_4^- or Cl^-) and frame walls can be decomposed using many-body decomposition:

$$\Delta E_{adsorption} = \Delta E_{deform}^{NKMOF-2} + \Delta E_{deform}^{CO_2} + \Delta E_{binding}^{CO_2+Anion} + \Delta E_{binding}^{CO_2+Frame\ wall} +$$

where ΔE_{deform}^{AF} is the deformation energy of the empty **NKMOF-2** before and after adsorption，$\Delta E_{deform}^{CO_2}$ is the deformation energy of CO_2 before and after adsorption，$\Delta E_{binding}^{CO_2+Anion}$ and $\Delta E_{binding}^{CO_2+Frame\ wall}$ are the binding energy of CO_2 and anions and CO_2 and the frame wall, $\Delta E_{3-body\ interactions}$ is the 3-body interaction. The energy decomposition results are shown in **Table S5**.

Table S1 Crystal data and refinement summary

Complex	**NKMOF-2-BF_4**
Formula	$C_{18}H_{12}BCl_2Cu_4F_4N_6O_6$
Formula weight	820.21
Crystal system	monoclinic
Space group	Cc
a (Å)	13.2703(4)
b (Å)	25.7082(7)
c (Å)	9.7839(9)
β (°)	92.398(6)
V (Å)^3	3334.9(3)
Z	4
D_c (g/cm^3)	1.634
R_{int}	5.96%
R_1 [$I > 2\sigma(I)$]	6.97%
wR_2 [$I > 2\sigma(I)$]	18.46%
GOOF	0.978
CCDC	1982349

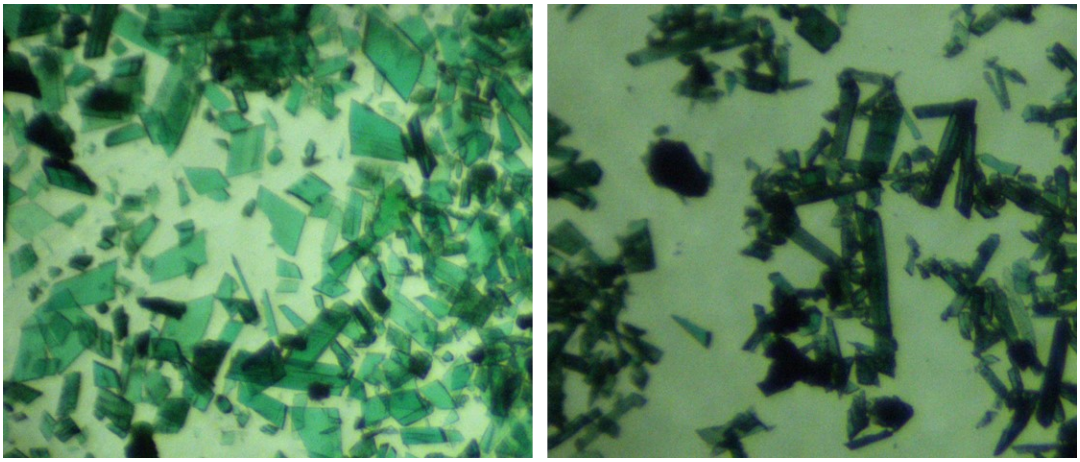

Fig. S1 Crystal Photographs of **NKMOF-2-Cl** (left) and **NKMOF-2-BF_4** (right).

Table S2 Use ion chromatography to determine the content of F and Cl in **NKMOF-2-BF_4**.

Sample	F content (wt %)	Cl content (wt %)
As calculated	9.27	8.65
As synthesized	7.83	8.75

Table S3 Use ion chromatography to determine the content of Cl in **NKMOF-2-Cl**.

Sample	Cl content (wt %)
As calculated	13.83
As synthesized	11.87

Table S4. Inductively Coupled Plasma Optical Emission Spectrometer (ICP-OES) for **NKMOF-2-BF_4**.

Sample	Cu content (wt %)	B content (wt %)
As-synthesized	32.6%	1.10%
Calculated	31.0%	1.21%

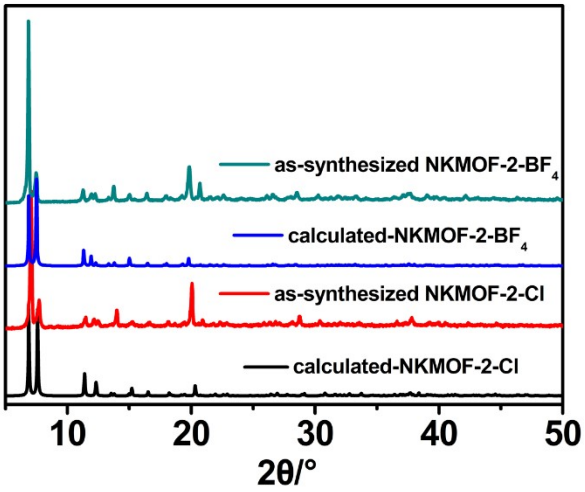

Fig. S2 The powder X-ray diffraction patterns for **NKMOF-2-Cl** and **NKMOF-2-BF_4**.

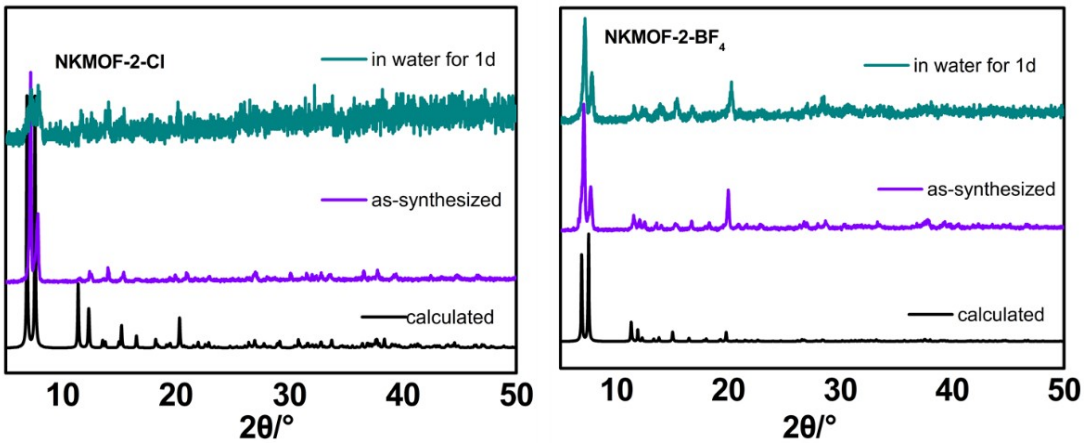

Fig. S3. PXRD patterns **of NKMOF-2-Cl** (left) and **NKMOF-2-BF_4** (right) as-synthesized and soaked in water for 1 day.

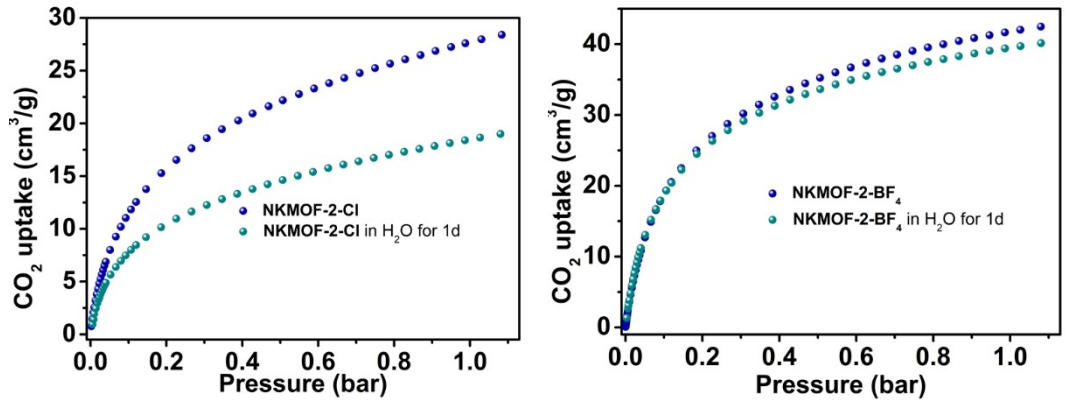

Fig. S4 CO_2 adsorption of **NKMOF-2-Cl** (left) and **NKMOF-2-BF$_4$** (right) at 298K. As-synthesized (royal blue), soaking in water for 1day (dark cyan).

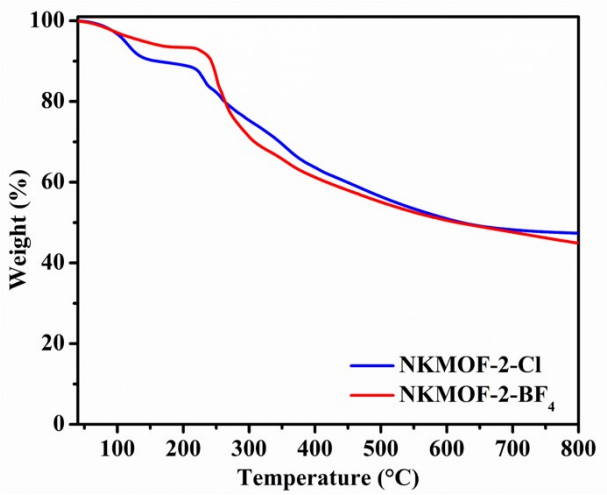

Fig. S5 TGA curves for **NKMOF-2-Cl** and **NKMOF-2-BF$_4$**.

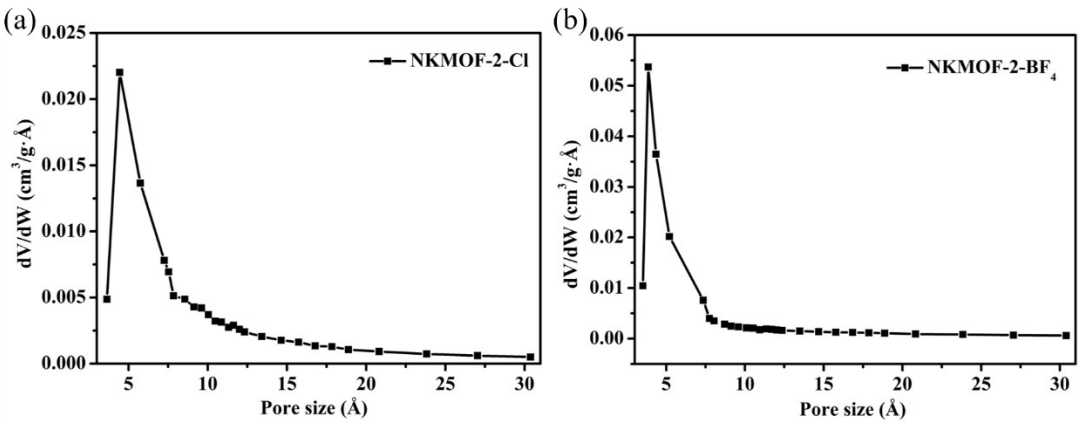

Fig. S6 Pore size distribution calculated based on CO_2 adsorption isotherms at 195 K

for **NKMOF-2-Cl** (a) and **NKMOF-2-BF_4** (b).

Table S5 The energy decomposition of the interactions between the CO_2, anion (BF_4^- or Cl^-), and frame walls, where AF represents Anion + Frame wall, C is CO_2, and FC represents Frame wall + CO_2. (Unit in kJ/mol)

		NKMOF-2-BF_4	**NKMOF-2-Cl**	**Difference**
Adsorption Energy		-59.7	-50.3	-9.4
Deformed energy	AF	-1.2	2.8	-4.0
	C	1.1	0.8	0.3
Binding energy	AC	11.6	16.8	-5.2
	FC	-74.0	-60.5	-13.5
	AF*	220.4	241.2	-20.8
3-body interactions		2.8	-10.2	13.0

Note: The AF binding energies are positive due to the arbitrary definitions of charged reference states, thus the value itself has no realistic physical meanings and we should only focus on the changes due to the influence of different anions.

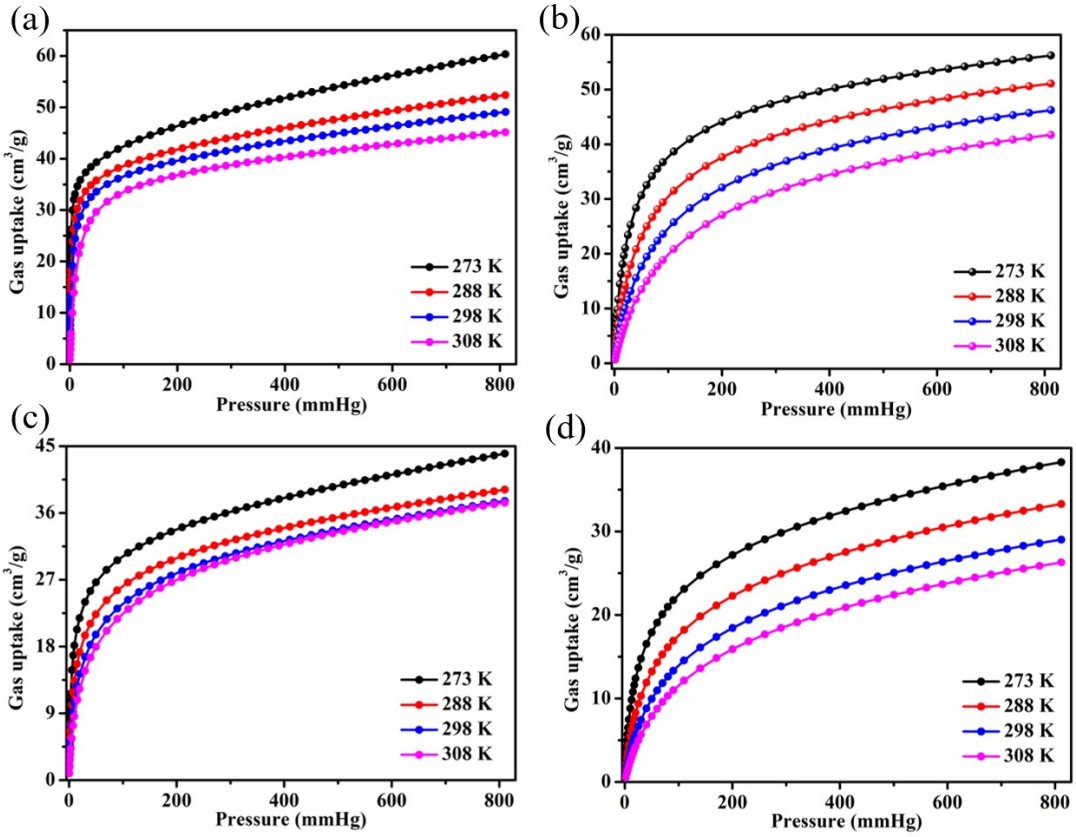

Fig. S7 Single-component adsorption isotherm at different temperatures for **NKMOF-2**. (a) C_2H_2 adsorption for **NKMOF-2-BF$_4$**; (b) CO_2 adsorption for **NKMOF-2-BF$_4$**; (c) C_2H_2 adsorption isotherms for **NKMOF-2-Cl**; (d) CO_2 adsorption isotherms for **NKMOF-2-Cl.**

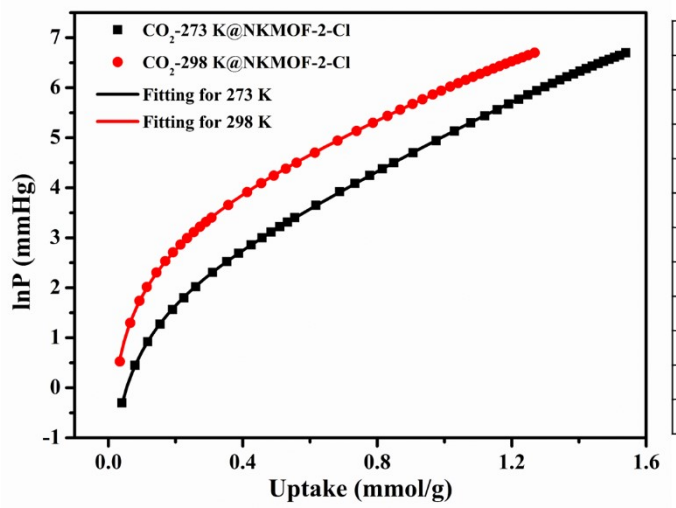

R^2	0.99998	
	Value	Standard Error
a0	-3508.9585	30.16566
a1	-776.81268	196.3777
a2	997.88585	347.89834
a3	785.3588	224.75448
a4	-647.65934	111.07781
a5	126.83765	28.32781
b0	15.6208	0.10508
b1	5.66534	0.67879
b2	-6.40803	1.16291
b3	1.23258	0.56829

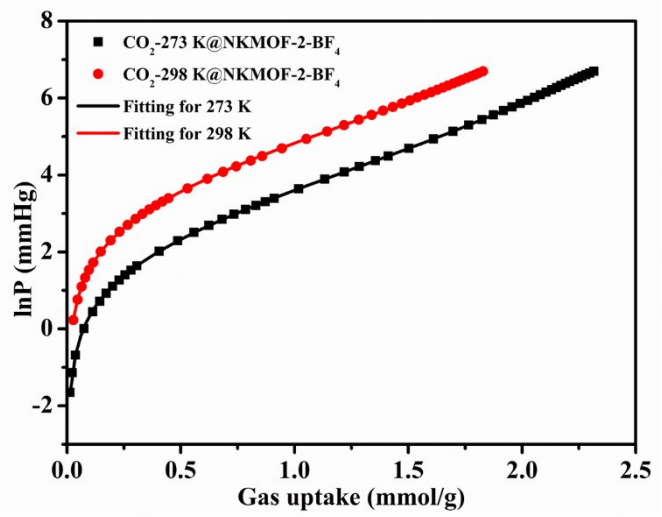

R^2	0.99997	
	Value	Standard Error
a0	-3955.45327	24.12285
a1	-469.70705	128.19228
a2	872.34996	166.43096
a3	-586.6357	71.51717
a4	178.13085	22.00368
a5	-28.63784	3.81801
b0	17.08697	0.08494
b1	2.09767	0.44868
b2	-1.72544	0.56982
b3	0.75784	0.19844

Fig. S8 The virial fitting of CO_2 sorption data for **NKMOF-2-Cl** (top) and **NKMOF-2-BF$_4$** (bottom).

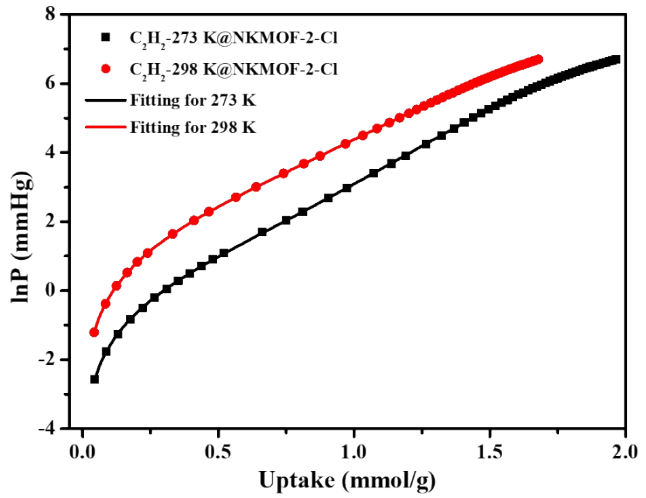

R^2	0.99998	
	Value	Standard Error
a0	-4593.94544	28.365
a1	-676.8184	141.53737
a2	493.02586	179.52779
a3	952.16721	86.91066
a4	-407.7971	39.85208
a5	41.60479	7.88249
b0	17.23858	0.0996
b1	5.77132	0.50083
b2	-4.85933	0.63153
b3	0.29772	0.22624

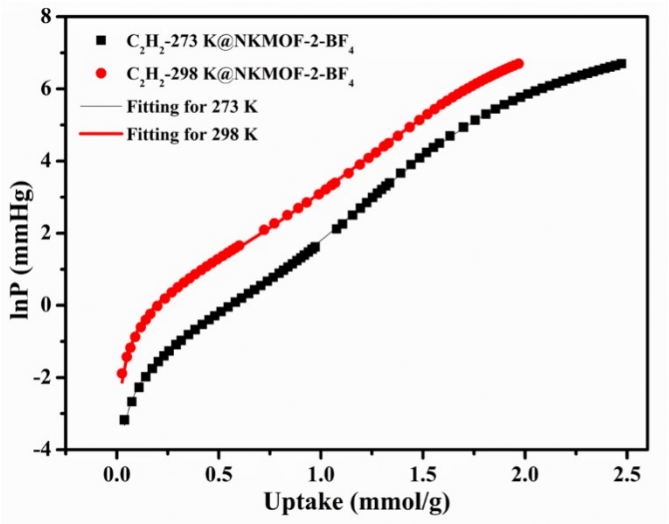

R^2	0.99979	
	Value	Standard Error
a0	-5179.37663	97.42195
a1	-69.66743	424.37617
a2	611.44566	500.29135
a3	840.90539	207.57342
a4	-642.11794	58.15298
a5	103.3847	9.38981
b0	18.89179	0.33761
b1	1.09819	1.45367
b2	-3.47757	1.64595
b3	1.17067	0.52659

Fig. S9 The virial fitting of C_2H_2 sorption data for **NKMOF-2-Cl** (top) and **NKMOF-2-BF$_4$** (bottom).

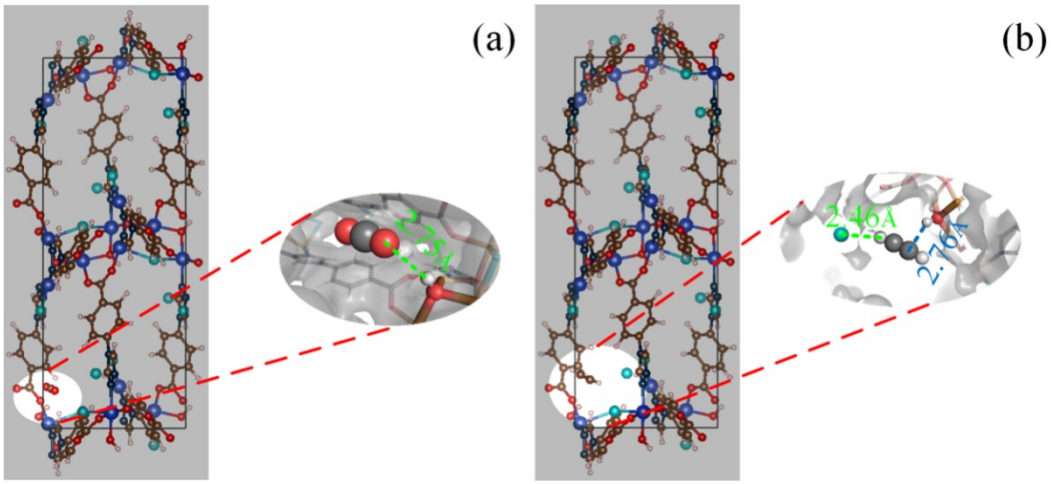

Fig. S10 The primary adsorption sites in **NKMOF-2-Cl** for (a) CO_2 and (b) C_2H_2.

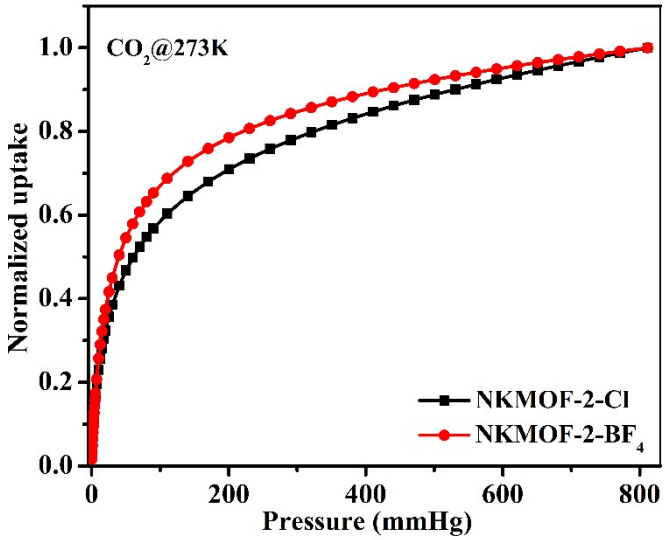

Fig. S11 The normalized CO_2 adsorption isotherms for **NKMOF-2-Cl** and **NKMOF-2-BF_4** at 273 K.

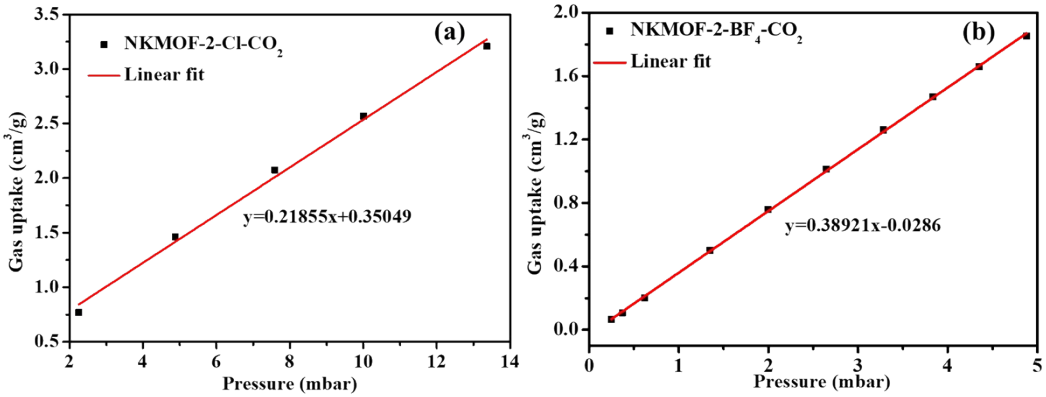

Fig. S12 The linear part of the adsorption profile of CO_2 for **NKMOF-2-Cl** (a) and **NKMOF-2-BF_4** (b) at 298 K

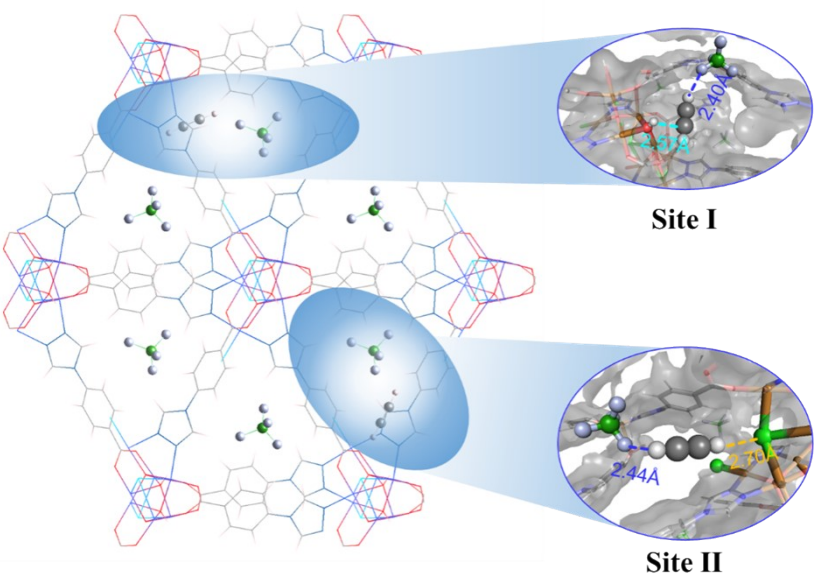

Fig. S13 The primary adsorption sites in **NKMOF-2-BF$_4$** for C_2H_2.

Table S6 The fitted parameters for the DSLF equation for the CO_2 adsorption isotherms for **NKMOF-2-Cl** and **NKMOF-2-BF$_4$** at 298 K.

Parameter	NKMOF-2-Cl	NKMOF-2-BF$_4$
$q_{A,sat}$ (mmol g^{-1})	0.75041	1.51733
b_A (kPa^{-1})	0.15996	0.14099
n_A	0.91138	0.92964
$q_{B,sat}$ (mmol g^{-1})	1.74498	1.52408
b_B (kPa^{-1})	0.01132	0.01449
n_B	0.82134	0.85267
R^2	0.9999947	0.999995

Table S7 The fitted parameters for the DSLF equation for the C_2H_2 adsorption isotherms for **NKMOF-2-Cl** and **NKMOF-2-BF$_4$** at 298 K.

Parameter	NKMOF-2-Cl	NKMOF-2-BF$_4$
$q_{A,sat}$ (mmol g^{-1})	1.14857	1.53393
b_A (kPa^{-1})	0.47049	1.64895
n_A	0.76221	0.93486
$q_{B,sat}$ (mmol g^{-1})	5.39573	6.09
b_B (kPa^{-1})	0.00665	0.00507
n_B	0.62382	0.67927
R^2	0.999983	0.999998

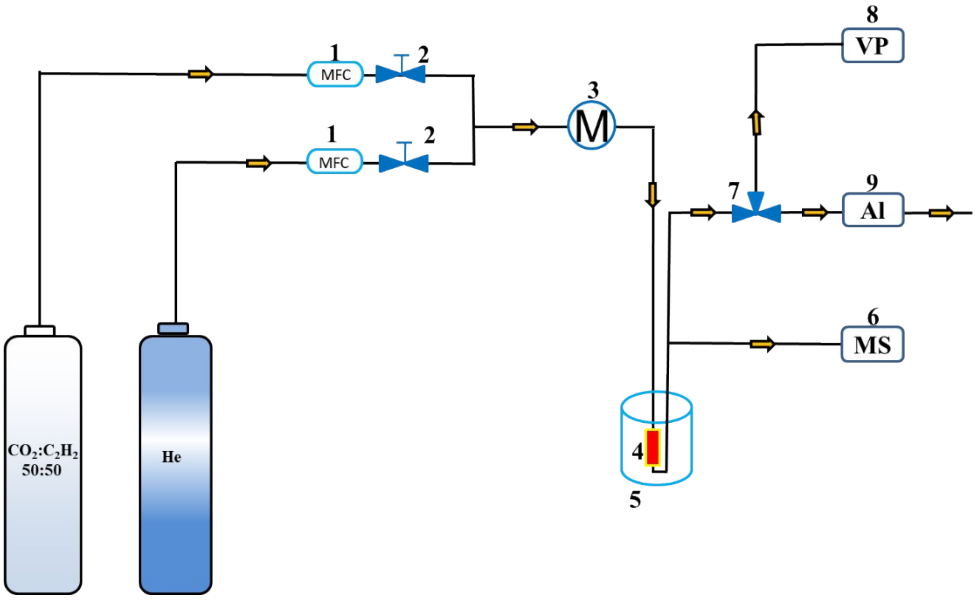

Fig. S14 The schematic breakthrough tests device. (1. Mass flow controller 2. Valve 3. Mixed gas room 4. Colum 5. Mantle heater 6. Mass spectrum 7. 3-way valve 8. Vacuum pump 9. Anti-backfire valve)

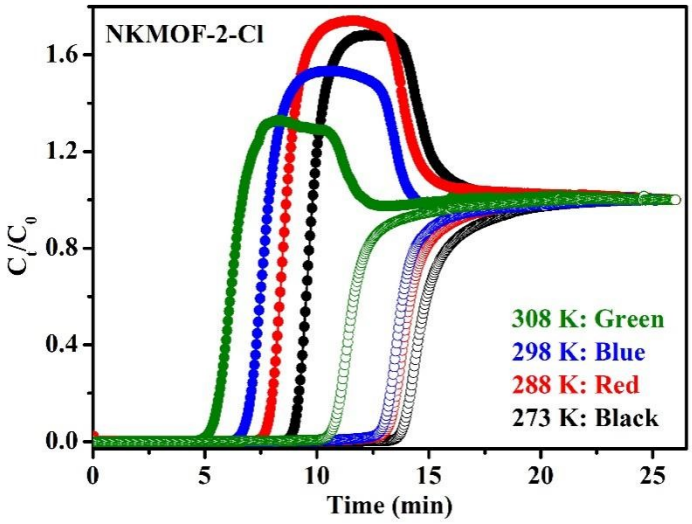

Fig. S15 The breakthrough curves of C_2H_2/CO_2 (v/v =2/1) with He as carrier gas for **NKMOF-2-Cl** at 273 K, 288 K, 298 K and 308 K.

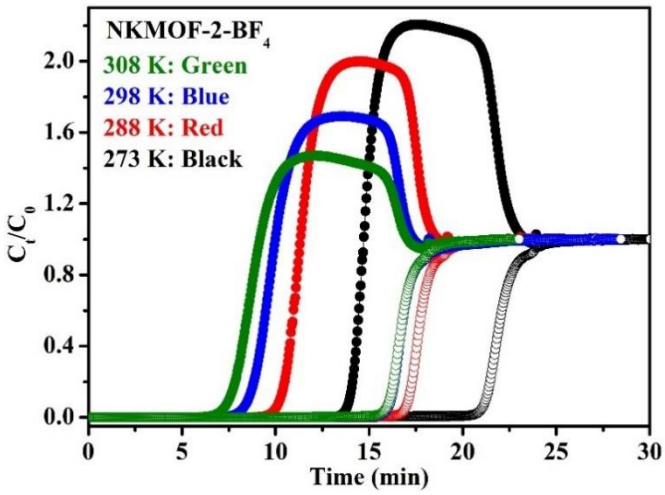

Fig. S16 The breakthrough curves of C_2H_2/CO_2 (v/v =2/1) with He as carrier gas for **NKMOF-2-BF_4** at 273 K, 288 K, 298 K and 308 K.

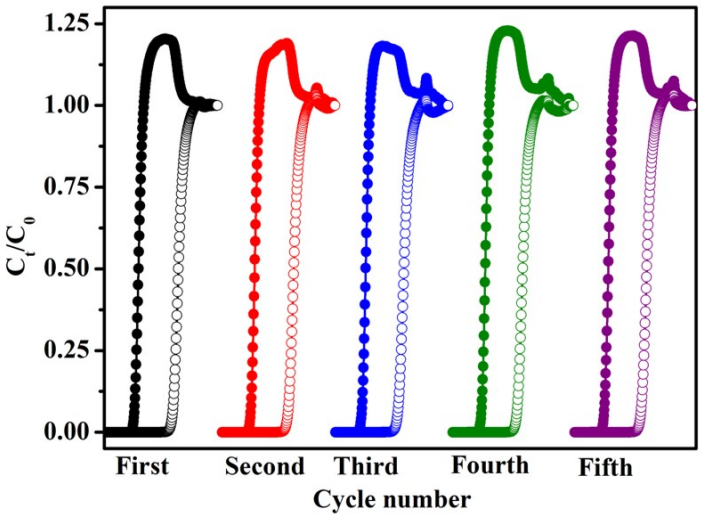

Fig. S17 The cyclic breakthrough curves of **NKMOF-2-Cl** in a fixed bed under the flow (10 cm^3/min) of C_2H_2/CO_2/He (10/10/80, v/v/v).

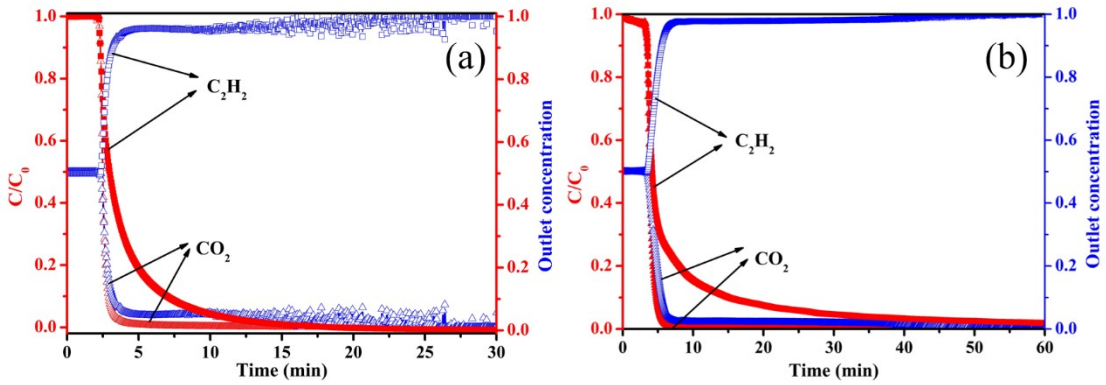

Fig. S18 The breakthrough desorption curves for **NKMOF-2-Cl** (a) and **NKMOF-2-BF_4** (b)

Table S8 The lattice parameters of **NKMOF-2-Cl** and **NKMOF-2-BF_4** from both DFT and experimental results.

	DFT Results		Experimental Results	
	NKMOF-2-Cl	**NKMOF-2-BF_4**	**NKMOF-2-Cl**	**NKMOF-2-BF_4**
a(Å)	13.19	13.38	13.1098(3)	13.2703(4)
b(Å)	26.23	26.16	25.6755(4)	25.7082(7)
c(Å)	10.07	9.86	9.7704(3)	9.7839(9)
β(º)	94.03	92.07	95.186(3)	92.398(6)
V(Å^3)	3476.34	3448.78	3275.26(14)	3334.9(3)

Table S9 The adsorption energies for CO_2 of the four primary adsorption sites in **NKMOF-2-BF_4** and **NKMOF-2-Cl**.

Adsorption Site	Adsorption energy (kJ/mol)	
	NKMOF-2-BF_4	NKMOF-2-Cl
I	-60.7	-60.3
II	-61.1	-50.9
III	-60.4	-52.4
IV	-60.3	-50.9

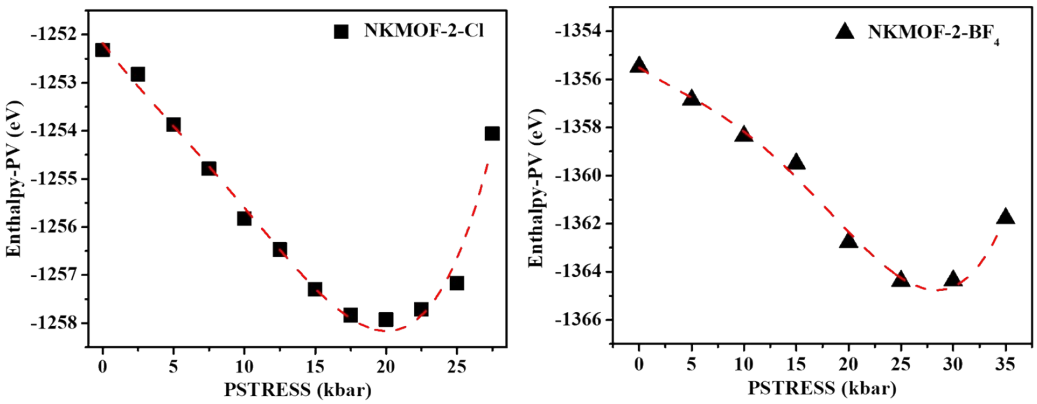

Fig. S19 The energy changing with increasing pulay stress.

Supplementary References

1. R. T. Yang, *Gas separation by adsorption processes*, Butterworth-Heinemann, 2013.

2. S. Lee, J. H. Lee and J. Kim, *Korean J. Chem. Eng.*, 2018, **35**, 214-221.

3. H. Zeng, M. Xie, T. Wang, R.-J. Wei, X.-J. Xie, Y. Zhao, W. Lu and D. Li, *Nature*, 2021, **595**, 542-548

4. G. Kresse and J. Hafner, *Phys. Rev. B.*, 1993, **47**, 558-561.

5. G. Kresse and J. Hafner, *Phys. Rev. B.*, 1994, **49**, 14251-14269.

6. G. Kresse and J. Furthmüller, *Phys. Rev. B.*, 1996, **54**, 11169-11186.

7. G. Kresse and J. Furthmüller, *Comput. Mater. Sci.*, 1996, **6**, 15-50.

8. J. Klimeš, D. R. Bowler and A. Michaelides, *J. Phys.: Condens. Matter*, 2009, **22**, 022201.

9. S. L. Dudarev, G. A. Botton, S. Y. Savrasov, C. J. Humphreys and A. P. Sutton, *Phys. Rev. B*, 1998, **57**, 1505-1509.